Journal of Computational Physics 229 (2010) 3415–3427

Contents lists available at ScienceDirect

Journal of Computational Physics

journal homepage: www.elsevier.com/locate/jcp

A fully conservative Eulerian–Lagrangian method for a convection–diffusion problem in a solenoidal field

Todd Arbogast [a,b,1], Chieh-Sen Huang [c,*]

[a] The University of Texas at Austin, Department of Mathematics, 1 University Station C1200, Austin, TX 78712, USA
[b] The University of Texas at Austin, Institute for Computational Engineering and Sciences, 1 University Station C0200, Austin, TX 78712, USA
[c] Department of Applied Mathematics and National Center for Theoretical Sciences, National Sun Yat-sen University, Kaohsiung 804, Taiwan, ROC

ARTICLE INFO

Article history:
Received 14 September 2009
Received in revised form 7 January 2010
Accepted 12 January 2010
Available online 20 January 2010

Keywords:
Advection–diffusion
Characteristics
Local conservation
ELLAM
Cellular flow
Divergence-free flow
Convection-enhanced diffusion

ABSTRACT

Tracer transport is governed by a convection–diffusion problem modeling mass conservation of both tracer and ambient fluids. Numerical methods should be *fully conservative*, enforcing both conservation principles on the discrete level. Locally conservative characteristics methods conserve the mass of tracer, but may not conserve the mass of the ambient fluid. In a recent paper by the authors [T. Arbogast, C. Huang, A fully mass and volume conserving implementation of a characteristic method for transport problems, SIAM J. Sci. Comput. 28 (2006) 2001–2022], a fully conservative characteristic method, the Volume Corrected Characteristics Mixed Method (VCCMM), was introduced for potential flows. Here we extend and apply the method to problems with a solenoidal (i.e., divergence-free) flow field. The modification is a computationally inexpensive simplification of the original VCCMM, requiring a simple adjustment of trace-back regions in an element-by-element traversal of the domain. Our numerical results show that the method works well in practice, is less numerically diffuse than uncorrected characteristic methods, and can use up to at least about eight times the CFL limited time step.

1. Introduction

We consider the numerical approximation of a convection–diffusion problem in a solenoidal field. The problem is a type of cellular flow. In the two-dimensional domain $\Omega = [0,1] \times [0,1]$, we seek $\phi(\mathbf{x},t) = \phi(x,y,t)$ as the solution to

$$\phi_t + \mathbf{u} \cdot \nabla\phi - \nabla \cdot \alpha\nabla\phi = F\phi \quad \text{for } \mathbf{x} \in \Omega,\ t > 0, \tag{1.1}$$

$$\phi(\mathbf{x},0) = \phi^0(\mathbf{x}) \quad \text{for } \mathbf{x} \in \Omega, \tag{1.2}$$

with a periodic boundary condition, where $\alpha(\mathbf{x}) \geqslant \alpha_* > 0$ and the vector field $\mathbf{u}(\mathbf{x})$ is itself periodic over Ω and solenoidal (i.e., divergence-free):

$$\nabla \cdot \mathbf{u} = 0 \quad \text{for } \mathbf{x} \in \Omega,\ t > 0. \tag{1.3}$$

The equations model convective transport of a tracer ϕ in an ambient fluid with velocity $\mathbf{u}$ (the term $\mathbf{u} \cdot \nabla\phi$) subject to diffusion (the term $-\nabla \cdot \alpha\nabla\phi$) and reactions (the term $F\phi$), all in the periodic cell Ω. Note that the tracer ϕ itself has no effect on the flow $\mathbf{u}$.

* Corresponding author. Tel.: +886 7 5252000; fax: +886 7 5253809.
E-mail addresses: arbogast@ices.utexas.edu (T. Arbogast), huangcs@math.nsysu.edu.tw (C.-S. Huang).

[1] This author was supported in part by US National Science Foundation Grant DMS-0713815 and the King Abdullah University of Science and Technology (KAUST) Academic Excellence Alliance program.

0021-9991/$ - see front matter © 2010 Elsevier Inc. All rights reserved.
doi:10.1016/j.jcp.2010.01.009

This problem arises in many applications. It is used as a simple model in the study of vortices in an incompressible fluid, and, more generally, to model diffusion of passive tracers in a periodic flow [12,14,18–20]. Two practical examples include simulation and modeling of combustion [24] and magnetohydrodynamics (MHD) [5,9,15,25].

Periodicity of ϕ and $\mathbf{u}$ arise in the applications, but, in fact, the numerical algorithm described herein does not require periodicity. Our algorithm would be formulated the same if we assumed no-flow boundary conditions ($\mathbf{u}\cdot\nu = 0$ and $\alpha\nabla\phi\cdot\nu = 0$ on $\partial\Omega$). However, for ease of exposition, we retain the periodicity assumptions.

Lagrangian moving mesh methods have been developed for problems like 1.1, 1.2 and 1.3 for a number of years (see, e.g. [6,26]). Similar to moving mesh methods, characteristic Eulerian–Lagrangian methods [2,8,11] have been applied to convection–diffusion problems since at least the 1980s. Recently, Liu et al. [17] applied a characteristic ELLAM scheme to the MHD problem. Such methods use operator splitting to separate the problem into transport, reaction, and diffusion steps. They use an Eulerian–Lagrangian framework, treating transport and reaction terms in a Lagrangian frame but diffusion in an Eulerian. We discuss mainly the transport step in this paper. The advantage of these methods is that large time steps can be used, since no CFL constraint arises for numerical stability of the transport part. This leads to approximations with less numerical diffusion than competing methods such as Godunov's method (see, e.g. [1]).

To maintain physical consistency of the numerical solution, the specific characteristic method used must in some way satisfy the local mass conservation principle numerically. Otherwise, loss or creation of mass over time will quickly destroy the solution. Such conservative characteristic methods have been known since the early 1990s [2,8]. However, it was recently pointed out by the authors [1] that it is critical to conserve locally the mass of *both* the transported fluid and the ambient fluid. We call such a method *fully conservative*.

Currently, the only fully conservative method, one that maintains the local mass conservation principles of both tracer and ambient fluids, is the volume corrected characteristics-mixed method (VCCMM) [1]. It is a modification of the ELLAM scheme called the characteristics-mixed method (CMM) [2], and it was developed and applied to problems with a potential (i.e., nonsolenoidal) velocity field $\mathbf{u}$. Very briefly, VCCMM computes the transport part of the problem on the computational mesh over a time step in three main steps. Step 1 is to trace (approximately) each mesh element E backward in time from the advanced time level to the previous time level along the characteristics or streamlines of the flow. Step 2 is then to correct the volume of the trace-back elements $\tilde{E}$ so each agrees with the volume of E (of course maintaining the property that the entire corrected trace-back mesh tessellates space). Finally, Step 3 is to sum the tracer mass in each $\tilde{E}$ at the previous time level. This mass is assumed transported to the original mesh element E at the advanced time level. Note that Step 3 ensures local mass conservation of the tracer. Because the volume of the trace-back element is corrected in Step 2, the sum of ambient and tracer mass is conserved, and so the overall VCCMM conserves locally the mass of both fluids. Step 2 is absent from the original CMM.

In this paper, we adapt and apply the VCCMM to our model problem 1.1, 1.2 and 1.3. Because the velocity $\mathbf{u}$ is not potential, the algorithm presented in [1] requires a mild modification, as described in the next section. In Section 3, we present three numerical examples that illustrate the method and show its advantages. Namely, we can use large time steps, and we observe less numerical diffusion for the fully conservative scheme as compared to one conserving only the tracer mass. Finally, our conclusions are noted in Section 4.

2. The numerical method

Suppose we have a sequence of time levels $0 = t^0 < t^1 < \cdots$ at which we wish to compute the solution. We work over the time step t^n to t^{n+1}. We use a standard operator splitting technique [10] to decompose the problem (1.1) in time into the following three main steps.

Transport step. Given ϕ at time t^n, we solve for ϕ_1 over the time step

$$\phi_t + \mathbf{u}\cdot\nabla\phi = 0 \tag{2.1}$$

using our modified VCCMM. We give the details later in this section.

Reaction step. Given ϕ_1, we solve for ϕ_2 over the time step

$$\phi_t = F\phi. \tag{2.2}$$

This is a standard ordinary differential equation at each fixed $\mathbf{x}\in\Omega$. We may use several micro-time steps in the solution. Almost any reasonable numerical technique can be used here, so we will discuss it no further.

Diffusion step. Given ϕ_2, we solve for ϕ at time t^{n+1} over the time step

$$\phi_t - \nabla\cdot\alpha\nabla\phi = 0. \tag{2.3}$$

This is an elliptic partial differential equation. There are many techniques available to solve it. However, in keeping with our concerns for the transport step, a locally mass conservative method should be used. As a very incomplete list, these include, for example, mixed finite element methods [7,22], finite volume methods [3,23], and discontinuous Galerkin methods [4,15,21]. Any reasonable locally conservative method can be used here, so we do not discuss it further.

2.1. Characteristics and local mass conservation for transport

The characteristics of (2.1) describe the curves on which ϕ is constant. The characteristic trace-back $\check{\mathbf{x}}(t) = \check{\mathbf{x}}(\mathbf{x}; t)$ passing through $(\mathbf{x}, t^{n+1})$ satisfies the (time backward) differential equation

$$\frac{d\check{\mathbf{x}}}{dt} = \mathbf{u}(\check{\mathbf{x}}, t)), \quad t^n \leqslant t \leqslant t^{n+1}, \tag{2.4}$$

$$\check{\mathbf{x}}(t^{n+1}) = \mathbf{x}. \tag{2.5}$$

Let the domain Ω be partitioned into a set $\mathcal{T}$ of elements (i.e., subdomains that tessellate space). Let $E \in \mathcal{T}$ be an element, and define the space–time trace-back region of E from time t^{n+1} back to t^n as

$$\mathcal{E} = \left\{(\check{\mathbf{x}}, t) \in \Omega \times [t^n, t^{n+1}] : \check{\mathbf{x}} = \check{\mathbf{x}}(\mathbf{x}, t) \text{ for } \mathbf{x} \in E\right\}.$$

Note that $E = \mathcal{E} \cap \{t^{n+1}\}$ and we define the trace-back region as

$$\check{E} = \{\check{\mathbf{x}} \in \Omega : \check{\mathbf{x}} = \check{\mathbf{x}}(\mathbf{x}, t^n) \text{ for } \mathbf{x} \in E\} = \mathcal{E} \cap \{t^n\}. \tag{2.6}$$

We tacitly use the periodicity of the problem in the above definitions (i.e., if $\check{\mathbf{x}}$ traces to $\partial\Omega$, it re-enters periodically). We remark in passing that, in the case of no-flow ($\mathbf{u} \cdot \nu = 0$) or even outflow ($\mathbf{u} \cdot \nu > 0$) boundary conditions, we never trace to $\partial\Omega$, so these conditions cause no difficulty for the method. We refer the interested reader to [1] for handling more general inflow boundary conditions.

Because of the spatial divergence-free condition (1.3), we can rewrite (2.1) as the space–time divergence

$$\phi_t + \mathbf{u} \cdot \nabla\phi = \nabla_{x,t} \cdot \begin{pmatrix} \phi\mathbf{u} \\ \phi \end{pmatrix} = 0. \tag{2.7}$$

Noting that no mass transports across the streamlines, integration over $\mathcal{E}$ and application of the divergence theorem to (2.7) leads to our *local mass conservation principle* for ϕ [2]. It is

$$\int_E \phi(\mathbf{x}, t^{n+1})\, d\mathbf{x} = \int_{\check{E}} \phi(\mathbf{x}, t^n)\, d\mathbf{x}, \tag{2.8}$$

which is the basis for our transport method.

However, the ambient fluid is also conserved, and thus also the total fluid; that is, (1.3) itself is

$$\nabla_{x,t} \cdot \begin{pmatrix} \mathbf{u} \\ 1 \end{pmatrix} = 0. \tag{2.9}$$

A similar computation leads to the *local volume conservation principle* [1]

$$|E| = |\check{E}|, \tag{2.10}$$

where $|S| = \int_S d\mathbf{x}$ is the volume (i.e., area) of a domain S.

2.2. VCCMM for transport

We begin the transport step by defining our computational mesh $\mathcal{T}$ that tessellates space. Unfortunately, given a mesh element $E \in \mathcal{T}$, it is not possible to trace points accurately according to (2.4) and (2.5), nor is it possible to fully resolve the boundary of the trace-back element $\check{E}$ of E. Therefore, in practice, one approximates $\check{E}$ by $\widetilde{E}$, in which one traces approximately, say, only the vertices and midpoints of E, and simply defines $\widetilde{E}$ to be a polygon connecting the points.

The collection of $\widetilde{E}$ continue to tessellate space, and the locally mass conservative method is to advance the tracer concentration in time according to the mass constraint (2.8). We approximate $\phi(\mathbf{x}, t^n)$ over the mesh by a piecewise constant function ϕ^n. We begin by projecting the initial condition into the mesh to give ϕ^0 and then, given ϕ^n, defining on E

$$\phi_E^{n+1}|E| = \int_{\widetilde{E}} \phi^n(\mathbf{x})\, d\mathbf{x}. \tag{2.11}$$

The problem is now manifest: Most likely the volume constraint (2.10) fails for $\widetilde{E}$, i.e., $|E| \neq |\widetilde{E}|$. Since $\widetilde{E}$ is only approximately $\check{E}$, we are at liberty to correct the volume error by perturbing the points defining $\widetilde{E}$, so that indeed

$$|\widetilde{E}| = |\check{E}| = |E|. \tag{2.12}$$

We remark that in practice, one can improve the accuracy of the method by postprocessing the piecewise constant function ϕ^n into a piecewise linear function prior to computing the integral in (2.11). Slope limiting may be necessary to avoid creating artificial local extrema (see, e.g., [2]). However, this was not done in the numerical results that follow.

2.3. VCCMM volume adjustment

As we will see in the next section, even small volume errors tend to build up into large errors over many time steps. In subsurface transport problems, in which the velocity is a potential flow arising from the application of Darcy's law, the initial, uncorrected volume errors are very large, and concentrated at the locations of the injection wells (for example, these errors can be as large as 200% [1]). Therefore, the original VCCMM algorithm contained a complex adjustment strategy involving three steps. (1) First, one traces particles forward out of the injection wells, and adjusts the volume of the region affected. (2) Second, between the wells, starting adjacent to the injection wells and moving towards the production wells, entire layers or rings of elements are adjusted so as to have the correct volume. Assuming the trace-back layer edge closest to an injector has been adjusted, the points on the far edge are adjusted simultaneously. These trace-back points are adjusted in the direction of the flow field, so that no bias is introduced into the *direction* of the overall flow. (3) Finally, the error within an adjusted layer of elements is now small, and individual elements are adjusted to have the correct volume by traversing the layer and adjusting the position of the midpoints.

On the other hand, solenoidal or divergence-free flows do not concentrate the volume errors. Numerical examples shown in the next section show volume errors more on the order of ±1e−3%. Therefore, a complex volume adjustment is not needed, and only something akin to step (3) is required. That is, we need only a simple element-by-element adjustment, leaving the vertices unperturbed and adjusting the locations of the midpoints. The only question is to decide the element adjustment order.

Perhaps the simplest strategy is to adjust the midpoints of each element in column-wise or row-wise fashion, as depicted in Fig. 2.1, where the original rather than the traceback mesh is shown for ease of visualization. Consider, for example column-wise adjustment. We begin on the bottom left element (Element 1 in the figure) by adjusting the top boundary midpoint (between Elements 1 and 2) so that the element volume (of Element 1) is correct. We then proceed upwards to the next element (Element 2) and adjust its top boundary midpoint until we reach the top of the domain. This top element is not yet adjusted for volume balance. Instead, we move to the next right column and repeat (for Elements 3–4, 5–6, and then 7–8). Finally, we adjust the right-hand side midpoints of the top row, starting from the left and working right (Elements 9–11). Note that the final element (Element 12) needs no adjustment, since the outer boundary condition (periodicity) implies that we maintain global volume conservation. This simple adjustment procedure often works very well and produces no systematic bias, since the initial volume errors observed are so small. The row-wise adjustment is similar. Obviously there are other, equally simple adjustment strategies that one might apply.

However, in some examples a systematic bias may result. The reason is that in some examples the volume errors tend to build up in the last few elements. This is especially true when large time steps are used, since the volume errors tend to be larger in that case. The goal is to traverse the domain in such a way that volume errors tend to cancel along the way. That is, we do not want to choose an element ordering that first treats $\widetilde{E}$ that are mostly too big, followed by elements mostly too small. The first too big $\widetilde{E}$ will push its volume into the next $\widetilde{E}$, making it even larger, which must in turn be pushed into the next $\widetilde{E}$, and so forth, until finally the too small elements are encountered.

We will see a staircase-like diagonal element-by-element adjustment in the next section (Example 1 with a large time step, used also in the other two examples with large time steps – see Fig. 3.7). One traverses the domain from the bottom-left to the upper-right corner along 45° lines from the bottom-left to the top-right.

3. Some numerical results

In this section we show by numerical examples that the volume correction step is a critical component in Lagrangian approximation of convection in a solenoidal field. Our examples apply to Eqs. (1.1) and (1.2). Recall that in all cases $\Omega = [0,1] \times [0,1]$. Except in one case, we turn off the reaction and diffusion, i.e., we set $F = 0$ and $\alpha = 0$, so we see only pure transport of the tracer.

We use rectangular grids for ease of implementation, though this is not necessary. All the ideas extend to unstructured triangular meshes, and even to more general arbitrary nonconforming tessellations of the domain into elements (although

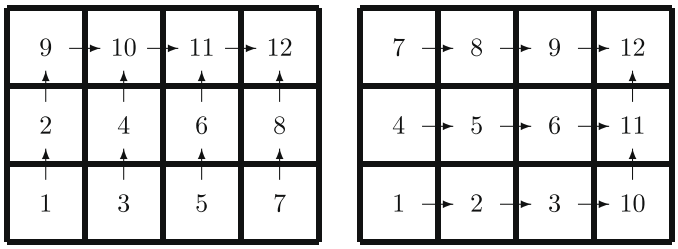

Fig. 2.1. Examples of column-wise (left) and row-wise (right) adjustment strategies on a simple rectangular grid, wherein we show the original grid rather than the traceback mesh. The numbers give the element volume adjustment order, and the arrows show the midpoint that is adjusted (the arrow pointing out is the one adjusted for that element).

the elements should probably be convex or nearly so). The only difficulty perhaps is to find an efficient trace-back tracking algorithm (see, e.g., [13,16]).

The basic Lagrangian methods found in the literature have no volume adjustment. A prototypical example is the Characteristics Mixed Method (CMM) [2], which we take as the baseline in our numerical results. We compare these to the VCCMM, which is the same method as CMM except for the addition of the volume correction step of Section 2.3. Thus our numerical results are strictly comparable, and show only the effect of volume conservation.

3.1. Example 1

For our first numerical example, We define $\mathbf{u}$ by

$$\mathbf{u} = \begin{pmatrix} -0.1 + 50\sin(2\pi x)\cos(2\pi y) \\ -50\cos(2\pi x)\sin(2\pi y) \end{pmatrix},$$

which is divergence-free and gives rise to the flow shown in Fig. 3.1. The initial condition is

$$\phi(x,y,0) = \begin{cases} 2, & 0.3 < x < 0.7 \quad \text{and} \quad 0.3 < y < 0.7, \\ 1, & \text{otherwise}, \end{cases} \tag{3.1}$$

which has a high concentration in a small square of width 0.4 in the center of the domain $(0,1)^2$.

We use a spatial grid of 256×256 and time step $\Delta t = 1\text{e}{-4}$, which is 2.56 times the CFL time step, defined as $\frac{h}{2u_{\max}}$, where h is the grid spacing and $u_{\max}$ is the maximal speed of the velocity $\mathbf{u}$. The initial, uncorrected volume error is depicted in Fig. 3.2 and varies from ±1.72e−3%. The scheme without volume adjustment, CMM, is subject to this volume error. The simple correction algorithm of Section 2.3 reduces these errors to the order of rounding error. Although the volume error is small in this problem, the error does build up over time, as can be seen in Fig. 3.3, which compares the tracer concentration ϕ for CMM and VCCMM. Our numerical data is summarized in Table 3.1.

It is clear that there is a big difference between the two methods. The results using a 512×512 grid and half the original time step ($\Delta t = 0.5\text{e}{-4}$) is shown in Fig. 3.4. The two methods' results are not nearly so dissimilar, and they indicate that VCCMM is more accurate. In fact, VCCMM on the coarser grid (Fig. 3.3) has similar resolution as CMM on the finer grid (Fig. 3.4). Therefore we conclude that VCCMM is the better scheme, since it produces accurate answers in lower resolution computations.

A careful examination of Fig. 3.4 shows that, in the case of the CMM, tracer fills the center of the flow cells due to a larger numerical diffusion instigated from the volume errors. This phenomenon is lessened when a finer grid is used, but not completely removed.

So far our time steps are relatively small, i.e., 2.56 times the CFL condition. We next increase the time step by a factor of 3 to 7.69 times of the CFL condition. We show these results in Fig. 3.5. On the left is VCCMM with a 256×256 grid and $\Delta t = 3\text{e}{-4}$, which should be compared to the right side of Fig. 3.3 with the same grid and $\Delta t = 1\text{e}{-4}$. On the right is VCCMM with a 512×512 grid and $\Delta t = 1.5\text{e}{-4}$, which is comparable to the right side of Fig. 3.4 with $\Delta t = 0.5\text{e}{-4}$. We see less numerical diffusion when we can take a longer time step.

In this set of numerical tests on the 256×256 grid, the maximum volume errors grow from 1.72e−3% to about 1.55e−2% when we raise the time step from 1e−4 to 3e−4. Although the volume error is still very small, a straight-forward row-wise horizontal then vertical element-by-element adjustment (see Section 2.3, i.e., Fig. 2.1) does not work. The reason is that the volume errors tend to build up in the last few elements. In this example, we instead used a staircase-like diagonal element-by-element adjustment from the bottom-left to the upper-right corner, as mentioned in Section 2.3 (see Fig. 3.7). In this method, we use a diagonal adjustment pattern from the bottom or left side of the domain until we reach the right or top of the domain. We then adjust the top row and right-most column.

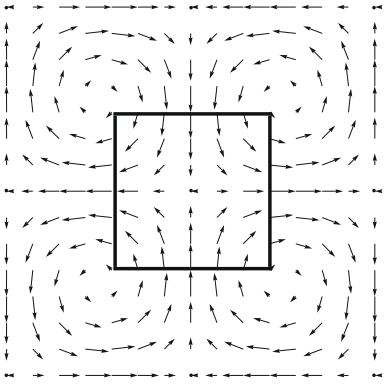

Fig. 3.1. Example 1: The velocity field, with the region occupied initially by the higher tracer concentration value.

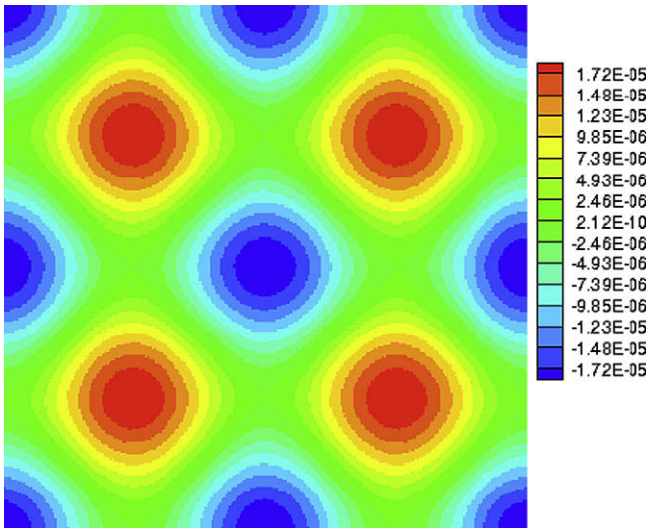

Fig. 3.2. Example 1: Initial, uncorrected volume errors using spatial mesh 256×256 and $\Delta t = 1e{-}4$. The variation is from ±1.72e-3%.

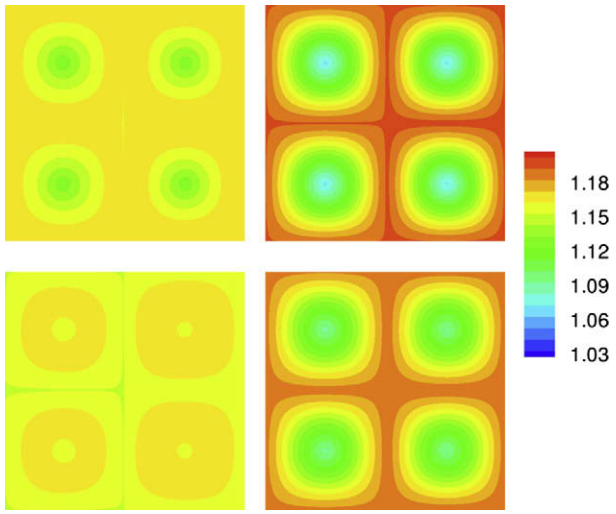

Fig. 3.3. Example 1: Tracer on 256×256 grid for CMM (left) and VCCMM (right) at time 0.3 (3000 steps, top) and 0.4 (4000 steps, bottom).

Table 3.1
Numerical data for various cases of Example 1.

$1/h$	Δt	Δt/CFL	Initial volume error	Adjustment pattern	Depicted in figure(s)
256	1.0e−4	2.56	±1.72e−5	column-wise	Fig. 3.3
512	0.5e−4	2.56	–	column-wise	Fig. 3.4
256	3.0e−4	7.69	±15.5e−5	diagonal	Figs. 3.5 and 3.6
512	1.5e−4	7.69	–	diagonal	Fig. 3.5

From the volume error plot (Fig. 3.2), it is easy to see the reason why we needed this adjustment strategy. If we adjust element-by-element in a horizontal strip, the error builds up at the very last element of the row, since the volume errors have the same sign along each x-strip (as does each y-strip, by the way). However, if we look at 45° angle strips, the volume errors take alternate signs, and they balance themselves along the strips. Therefore, the volume errors tend not to accumulate in the very last element, and we are able to use our relatively large time step.

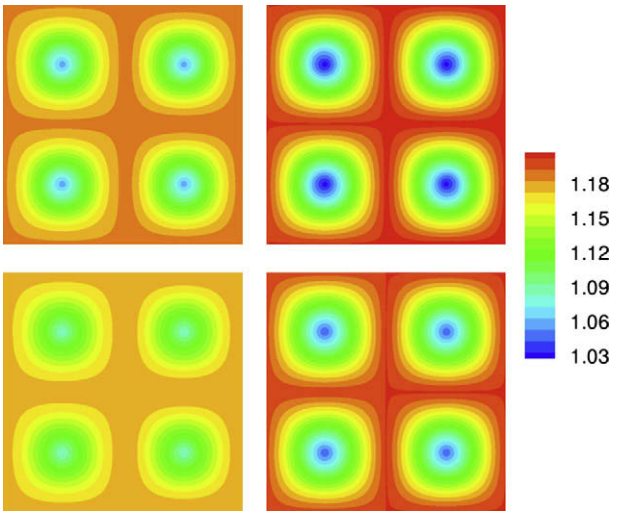

Fig. 3.4. Example 1: Tracer on 512×512 grid for CMM (left) and VCCMM (right) at time 0.3 (6000 steps, top) and 0.4 (8000 steps, bottom).

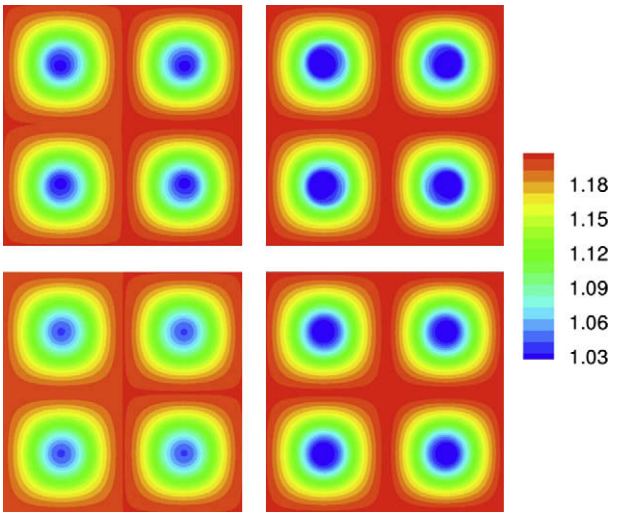

Fig. 3.5. Example 1: VCCMM tracer on 256×256 grid with $\Delta t = 3\text{e}{-4}$ (left) and on 512×512 grid with $\Delta t = 1.5\text{e}{-4}$ (right) at times 0.3 (top) and 0.4 (bottom).

Finally, it is instructive to note the level of detail that the method captures. Fig. 3.6 shows four snapshots of this problem at steps 10, 30, 60, and 80 with timestep $\Delta t = 3\text{e}{-4}$ on a 256×256 grid. Note the very low level of numerical diffusion that the fully conservative method is subject to.

3.2. Example 2

We next consider a problem with four eddies in its velocity field, taken from Weiss [25] and considered also in [17,26]. We note that the particular ELLAM method they use is *not* fully conservative, so it should suffer from the same volume error problem as CMM does. The velocity $\mathbf{u}$ is defined by

$$u_1(x,y) = \frac{\sin(4\pi x)}{4\pi}(2y(1-y)^2 - 2y^2(1-y)),$$
$$u_2(x,y) = -\cos(4\pi x)y^2(1-y)^2$$

and it is depicted by Fig. 3.8. We use the initial condition

$$\phi(x,y,0) = \begin{cases} 2, & 0.3 < y < 0.7, \\ 1, & \text{otherwise}. \end{cases}$$

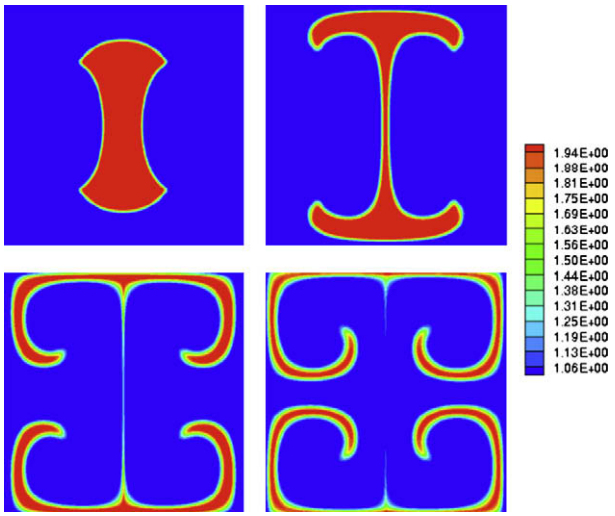

Fig. 3.6. Example 1: Evolution of the tracer concentration at early times on a 256×256 grid. Shown are steps 10, 30, 60, and 80 with $\Delta t = 3e{-}4$. Colors vary from 1.06 (blue) to 1.94 (red). (For interpretation of the references to color in this figure legend, the reader is referred to the web version of this article.)

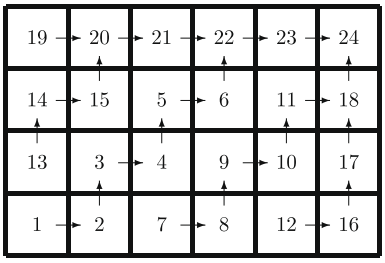

Fig. 3.7. A staircase-like diagonal element-by-element adjustment strategy from the bottom-left to the upper-right corner on a simple rectangular grid, wherein we show the original grid rather than the traceback mesh. The numbers give the element volume adjustment order, and the arrows show the midpoint that is adjusted (the arrow pointing out is the one adjusted for that element).

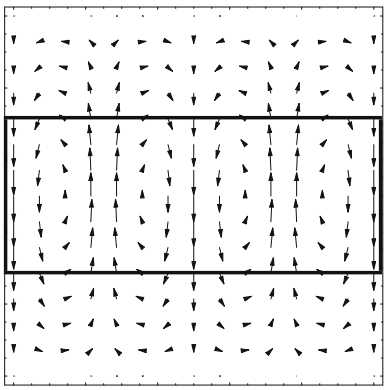

Fig. 3.8. Example 2: The velocity field, showing its four eddies, with the region occupied initially by the higher tracer concentration value.

Our numerical data is summarized in Table 3.2. For a spatial grid of 128×128 and time step $\Delta t = 0.1$, which is the 1.6 times the CFL time step, the initial volume error (see Fig. 3.9) is at the magnitude of 1.09e−3%, which, even though very small, is significant over many steps. Fig. 3.10 shows a comparison of the uncorrected CMM and the fully conservative VCCMM (using simple column-wise adjustment) concentration at step 3000, i.e., time 300. On the left-hand side we plot

Table 3.2
Numerical data for various cases of Example 2.

$1/h$	Δt	Δt/CFL	Initial volume error	Adjustment pattern	Diffusion α	Depicted in figure(s)
128	0.1	1.6	±1.0e−5	Column-wise	0	Fig. 3.10
128	0.5	8.0	±30.e−5	Diagonal	0	Figs. 3.12 and 3.13
128	0.5	8.0	±30.e−5	Diagonal	0.01	Fig. 3.14

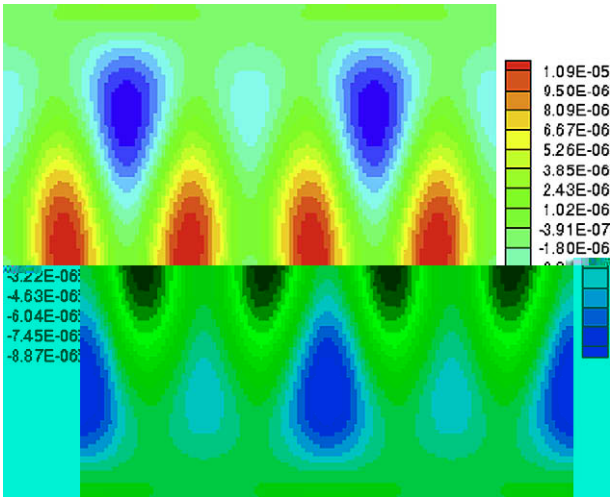

Fig. 3.9. Example 2: Initial, uncorrected volume errors for 128×128 mesh and $\Delta t = 0.1$. The variation is from −0.887e−3% to 1.09e−3%.

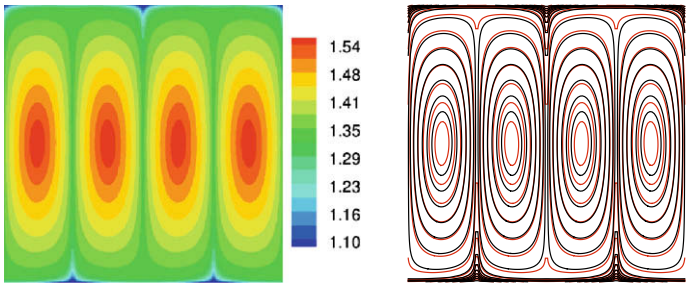

Fig. 3.10. Example 2: At time 300, (left) the VCCMM tracer concentration, and (right) corresponding concentration contours for VCCMM (in red) and CMM (in black). (For interpretation of the references to color in this figure legend, the reader is referred to the web version of this article.)

in color the VCCMM concentration between 1.10 (blue[2]) and 1.54 (red). Corresponding contour lines are plotted on the right-hand side for both VCCMM (in red) and CMM (in black). As can be seen easily, the red ovals (VCCMM) are much smaller than the black ovals (CMM), so VCCMM exhibits less numerical diffusion.

We next attempt to lengthen the time step. We use the same spatial grid of 128×128, but now the time step $\Delta t = 0.5$, which is eight times of the CFL condition. The maximum initial volume errors grow from 1e−3% to about 3e−2% (see Fig. 3.11). As before, a staircase-like diagonal type of element-by-element adjustment removes the volume error easily.

In Fig. 3.12, the black concentration contours use the previous $\Delta t = 0.1$, which takes 3000 steps to time $t = 300$, while the red contours are for $\Delta t = 0.5$, which takes only 600 steps to the final time. One can see easily that the red ovals ($\Delta t = 0.5$) are much smaller than the black ovals ($\Delta t = 0.1$), so again we see less numerical diffusion whenever we can take a larger time step.

Finally, we consider the problem with nonzero physical diffusion, i.e., (1.1) with $\alpha = 0.01$. Compared to Fig. 3.10 (left), the physical diffusion in Fig. 3.14 is apparent, especially near the bottom and top of the domain, i.e., at $y = 0$ and $y = 1$.

[2] For interpretation of color in Fig. 3.9, the reader is referred to the web version of this article.

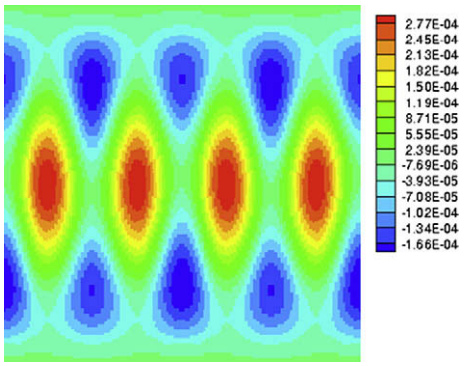

Fig. 3.11. Example 2: Initial, uncorrected volume errors for 128×128 mesh and $\Delta t = 0.5$. The variation is from $-1.66e{-}12\%$ to $2.77e{-}2\%$.

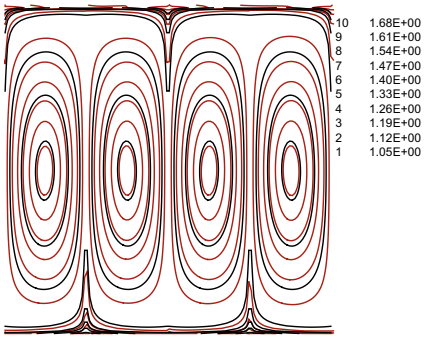

Fig. 3.12. Example 2: VCCMM contours for $\Delta t = 0.1$ (black) and $\Delta t = 0.5$ (red) at $t = 300$, i.e., using 3000 and 600 time steps, respectively. (For interpretation of the references to color in this figure legend, the reader is referred to the web version of this article.)

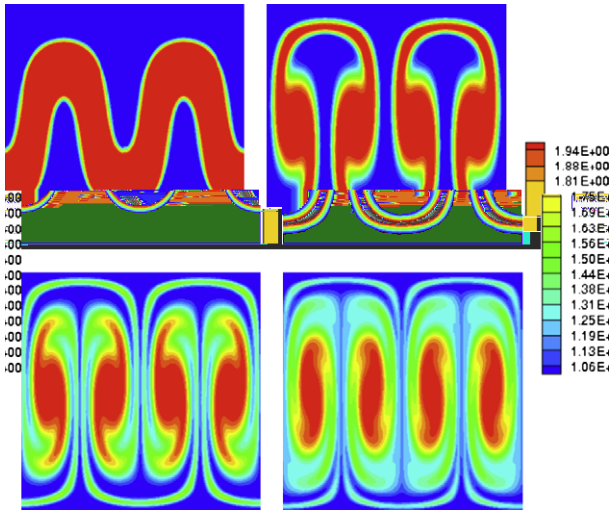

Fig. 3.13. Example 2: Evolution of the tracer concentration at early times on a 128×128 grid. Shown are steps 10, 30, 60, and 80 with $\Delta t = 0.5$. Colors vary from 1.06 (blue) to 1.94 (red). (For interpretation of the references to color in this figure legend, the reader is referred to the web version of this article.)

3.3. Example 3

Lastly, we show a numerical example with a time-dependent vector field. We modify $\mathbf{u}$ from Example 1 to

$$\mathbf{u} = \begin{pmatrix} -0.1 + 50\,\sin(2\pi x + 0.4\cos(50t))\cos(2\pi y) \\ -50\cos(2\pi x + 0.4\cos(50t))\sin(2\pi y) \end{pmatrix}, \tag{3.2}$$

and we use the same initial condition (3.1) as in Example 1.

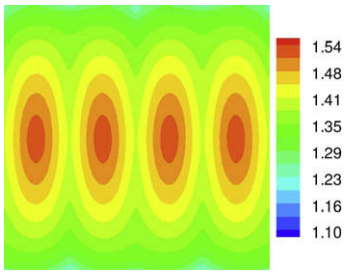

Fig. 3.14. Example 2: VCCMM tracer concentration at time 300 with physical diffusion $\alpha = 0.01$ (on a 128×128 grid with $\Delta t = 0.5$).

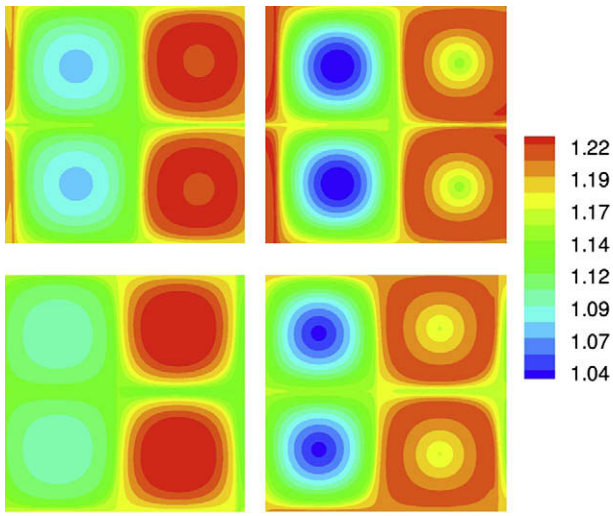

Fig. 3.15. Example 3: Tracer on 256×256 grid for CMM (left) and VCCMM (right) at time 0.3 (3000 steps, top) and 0.4 (4000 steps, bottom).

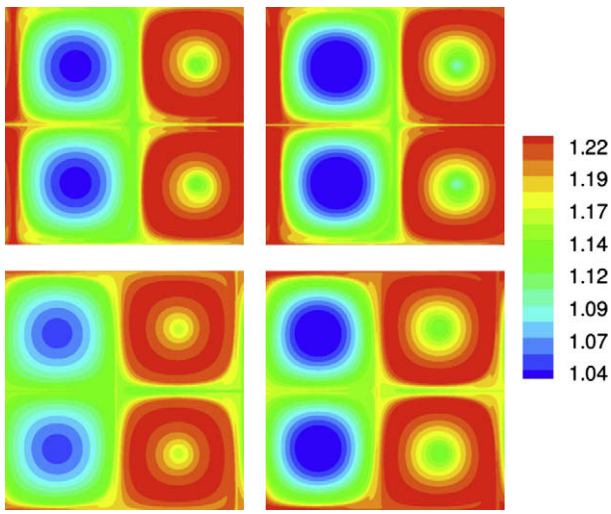

Fig. 3.16. Example 3: Tracer on 512×512 grid for CMM (left) and VCCMM (right) at time 0.3 (6000 steps, top) and 0.4 (8000 steps, bottom).

In Fig. 3.15, we see clear differences between CMM and VCCMM (with simple column-wise adjustment) using a 256×256 grid and Δt = 1e−4. Refinement to a 512×512 grid and Δt = 5e−5 in Fig. 3.16 shows that VCCMM gives the more accurate result, and that with CMM, the tracer fills the cells due to larger numerical diffusion.

Finally, we note that we also ran relatively large time steps for this problem. The staircase-like diagonal adjustment procedure (Section 2.3 and Fig. 3.7) worked well in removing any volume error; however, a time shift was necessary. For the time-independent problem (Example 1), the adjustment starts at element (1,1) on a domain $n \times n$, $n = 256$ or 512, proceeds to the line containing (2,1) and (1,2), and then to the line (3,1), (2,2), and (1,3), etc. Now for the time-dependent problem, the contours, and so also the volume errors, shift a bit to the right in time, as can be seen in Figs. 3.15 and 3.16. Thus we need to take the starting point for the adjustment algorithm at $(a,1)$, where the offset a, $1 \leqslant a \leqslant n$, depends on time. From (3.2), we see that a should be the solution of $2\pi(a-1)/n + 0.4\cos(50t) = 0$.

4. Conclusions

In this paper, we have described the Volume Corrected Characteristics Mixed Method (VCCMM) [1], which enforces local mass conservation of both the tracer and ambient fluids in transport problems with a velocity governed by a potential. A simple modification was presented to extend the definition of the VCCMM to solenoidal flows. The modification is actually a simplification of the original VCCMM, requiring adjustment of trace-back regions $\widetilde{E}$ in an element-by-element traversal of the domain, so that each $\widetilde{E}$ has the volume of the original mesh element E. Often a simple column-wise or row-wise adjustment suffices, but in other cases a better ordering is necessary. The traversal path should be chosen so that local volume errors tend to cancel along the way.

Our numerical results show that the method works well in practice, and better than uncorrected characteristic methods, such as the Characteristics Mixed Method (CMM) [2], which are more numerically diffuse than corrected versions. In fact, the corrected algorithm on a coarse grid can attain a similar level of resolution as the uncorrected algorithm on a fine grid.

The main advantage of characteristic methods is that, in principle, one may use large time steps. This has the effect of reducing mesh projection errors, and ultimately reducing numerical diffusion. However, the volume error grows with the time step. In uncorrected characteristic methods, one cannot use too large a time step before the numerical diffusion due to volume nonconservation degrades the solution. The volume correction step rectifies this difficulty in practice, and we showed examples using up to eight times the CFL limited time step.

There are many locally mass conservative characteristic methods available that only conserve the tracer mass. Our results show that they can benefit from the computationally inexpensive local volume correction adjustment procedure presented here.

Acknowledgment

The authors thank Professor James Nolen for helpful discussions regarding the applications of this work.

References

[1] T. Arbogast, C. Huang, A fully mass and volume conserving implementation of a characteristic method for transport problems, SIAM J. Sci. Comput. 28 (2006) 2001–2022.
[2] T. Arbogast, M.F. Wheeler, A characteristics-mixed finite element method for advection dominated transport problems, SIAM J. Numer. Anal. 32 (1995) 404–424.
[3] T. Arbogast, M.F. Wheeler, I. Yotov, Mixed finite elements for elliptic problems with tensor coefficients as cell-centered finite differences, SIAM J. Numer. Anal. 34 (1997) 828–852.
[4] D. Arnold, F. Brezzi, B. Cockburn, L. Marini, Unified analysis of discontinuous Galerkin methods for elliptic problems, SIAM J. Numer. Anal. 39 (2001/2002) 1749–1779.
[5] D.S. Balsara, D.S. Spicer, A staggered mesh algorithm using high order Godunov fluxes to ensure solenoidal magnetic fields in magnetohydrodynamic simulations, J. Comput. Phys. 149 (1999) 270–292.
[6] G. Beckett, J.A. Mackenzie, A. Ramage, D.M. Sloan, Computational solution of two-dimensional unsteady PDEs using moving mesh methods, J. Comput. Phys. 182 (2002) 478–495.
[7] F. Brezzi, M. Fortin, Mixed and Hybrid Finite Element Methods, Springer-Verlag, New York, 1991.
[8] M.A. Celia, T.F. Russell, I. Herrera, R.E. Ewing, An Eulerian–Lagrangian localized adjoint method for the advection–diffusion equation, Adv. Water Res. 13 (1990) 187–206.
[9] P.A. Davidson, An Introduction to Magnetohydrodynamics, Cambridge University Press, 2001.
[10] C. Dawson, M.F. Wheeler, An operator-splitting method for advection–diffusion–reaction problems, in: J.A. Whiteman (Ed.), MAFELAP Proceedings VI, Academic Press, 1988, pp. 463–482.
[11] J. Douglas Jr., T.F. Russell, Numerical methods for convection-dominated diffusion problems based on combining the method of characteristics with finite element or finite difference procedures, SIAM J. Numer. Anal. 19 (1982) 871–885.
[12] A. Fannjiang, G. Papanicolaou, Convection-enhanced diffusion for periodic flows, SIAM J. Appl. Math. 54 (1994) 333–408.
[13] R.W. Healy, T.F. Russell, Analytical tracking along streamlines in temporally linear Raviart–Thomas velocity fields, in: Bentley et al. (Eds.), Computational Methods in Water Resources XIII, vol. 2, A.A. Balkema, Rotterdam, 2000, pp. 631–638.
[14] A.P. Itin, R. de la Llave, A.I. Neishtadt, A. Vasiliev, Transport in a slowly perturbed convective cell flow, Chaos 12 (2002) 1043–1053.
[15] F. Li, C.W. Shu, Locally divergence-free discontinuous Galerkin methods for MHD equations, J. Sci. Comput. 22/23 (2005) 413–442.
[16] J. Liu, H. Chen, R. Ewing, G. Qin, An efficient algorithm for characteristic tracking on two-dimensional triangular meshes, Computing 80 (2007) 121–136.
[17] J. Liu, S. Tavener, H. Chen, ELLAM for resolving the kinematics of two-dimensional resistive magnetohydrodynamic flows, J. Comput. Phys. 227 (2007) 1372–1386.
[18] A. Majda, P. Kramer, Simplified models for turbulent diffusion: theory, numerical modeling, and physical phenomena, Phys. Reports 314 (1999) 237–574.
[19] J. Nolen, J. Xin, A variational principle based study of KPP minimal front speeds in random shears, Nonlinearity 18 (2005) 1655–1675.

[20] J. Nolen, J. Xin, Asymptotic spreading of KPP reactive fronts in incompressible space–time random flows, Annales de l'institut Henri Poincaré – Analyse Non Lineaire 26 (2008) 815–839.
[21] B. Rivière, M. Wheeler, V. Girault, A priori error estimates for finite element methods based on discontinuous approximation spaces for elliptic problems, SIAM J. Numer. Anal. 39 (2001) 902–931.
[22] J.E. Roberts, J.-M. Thomas, Mixed and hybrid methods, in: P.G. Ciarlet, J.L. Lions (Eds.), Handbook of Numerical Analysis, Finite Element Methods (Part 1), vol. 2, Elsevier Science Publishers B.V., North-Holland, Amsterdam, 1991, pp. 523–639.
[23] T.F. Russell, M.F. Wheeler, Finite element and finite difference methods for continuous flows in porous media, in: R.E. Ewing (Ed.), The Mathematics of Reservoir Simulation, Frontiers in Applied Mathematics, vol. 1, Society for Industrial and Applied Mathematics, Philadelphia, 1983, pp. 35–106 (Chapter II).
[24] N. Vladimirova, P. Constantin, A. Kiselev, O. Ruchayskiy, L. Ryzhik, Flame enhancement and quenching in fluid flows, Combust. Theory Modell. 7 (2003) 487–508.
[25] N.O. Weiss, The expulsion of magnetic flux by eddies, Proc. Roy. Soc. A 293 (1966) 310–328.
[26] P.A. Zegeling, On resistive MHD models with adaptive moving meshes, J. Sci. Comput. 24 (2005) 263–284.